Precision Genome Editing Using Bacteriophage-derived Peptides

Yan-ru Cui[1,4,5], Shao-jie Wang[1,5], Jun Chen[2], Jie Li[1,4], Wenzhang Chen[1], Shuyue Wang[1], Bing Meng[1], Wei Zhu[1], Zhuhong Zhang[3], Bei Yang[1], Biao Jiang[1], Guang Yang[1], Peixiang Ma[1,*], Jia Liu[1,6*]

[1]Shanghai Institute for Advanced Immunochemical Studies, ShanghaiTech University, Shanghai, 201210, China.

[2]College of Life Sciences, Zhejiang University, Hangzhou, Zhejiang, 310058, China.

[3]School of Pharmacy, Key Laboratory of Molecular Pharmacology and Drug Evaluation (Yantai University), Ministry of Education, Collaborative Innovation Center of Advanced Drug Delivery System and Biotech Drugs in Universities of Shandong, Yantai University, 264005, Yantai, Shandong, People's Republic of China.

[4]University of Chinese Academy of Sciences, Beijing, China.

[5] These authors contributed equally to this work.

[6]Lead Contact

*Correspondence should be addressed to: J. Liu (liujia@shanghaitech.edu.cn) and P. Ma (mapx@shanghaitech.edu.cn)

Highlights

- Periplasmic domain of phage major coat protein G8P ($G8P_{PD}$) inhibits SpyCas9
- $G8P_{PD}$ interferes with SpyCas9-sgRNA assembly in an allosteric manner
- $G8P_{PD}$ inhibits the genome-editing activity of SpyCas9 in human cells
- Timed delivery of $G8P_{PD}$ improves the editing specificity of constitutively expressed SpyCas9

SUMMARY

Protein and small molecule-based CRISPR inhibitors have been developed as selective off-switches to modulate CRISPR-Cas activity. These anti-CRISPR agents have important therapeutic implications because of their capability to improve the specificity of CRISPR-Cas in human cells. In this study, we reported the discovery of Cas9-inactivating peptides from inoviridae bacteriophages. These peptides, derived from the periplasmic domain of phage major coat protein G8P ($G8P_{PD}$), can inhibit the *in vitro* cleavage activity of purified *Streptococcus pyogenes* Cas9 (SpyCas9) proteins in an allosteric manner. Ectopic expression of full-length G8P ($G8P_{FL}$) or $G8P_{PD}$ in human cells can inactivate the genome-editing activity of SpyCas9 with minimum alterations of the mutation patterns. Most importantly, timed delivery of $G8P_{PD}$ can reduce the off-target activity of co-transfected SpyCas9 without compromising its on-target activity. Therefore, the G8Ps discovered in the current study represent the first anti-CRISPR peptides that can improve the specificity of constitutively expressed SpyCas9, implying the potential applications of G8Ps for precision genome editing.

INTRODUCTION

Clustered Regularly-Interspaced Short Palindromic Repeats (CRISPR) is the bacterial adaptive immune system to defend bacteriophage infections (Barrangou et al., 2007; Brouns et al., 2008; Marraffini and Sontheimer, 2008). During infection, invader DNA is captured and integrated into bacterial genome as CRISPR array. Sequences from CRISPR array are transcribed and processed into CRISPR RNAs (crRNAs), which direct CRISPR-associated (Cas) proteins to foreign nucleic acids (Barrangou et al., 2007; Brouns et al., 2008).

Type II CRISPR-Cas systems function with streamlined components comprising of a single nuclease protein such as Cas9 (Jinek et al., 2012). The modular and programmable features make CRISPR-Cas9 one of the most widely used tools for genome engineering applications (Cho et al., 2013; Cong et al., 2013; Jinek et al., 2013; Mali et al., 2013). However, CRISPR-Cas9 is associated with off-target cleavage (Koo et al., 2015), chromosomal rearrangement (Kosicki et al., 2018) and genotoxicity (Li et al., 2018b). These side effects mainly arise from the excessive or prolonged expression of CRISPR-Cas9 (Fu et al., 2014; Hsu et al., 2013; Pattanayak et al., 2013). As a therapeutic agent, SpyCas9 is often constitutively expressed in host cells (Fellmann et al., 2017), making the elevated activity of SpyCas9 a major safety concern. Temporal control of SpyCas9 activity have been investigated as an approach to improving its specificity in human cells. Technologies enabling the temporal control of SpyCas9 include optogenetic tools, intein splicing system and small molecule inducers or inhibitors (Cao et al., 2016; Maji et al., 2019; Nihongaki et al., 2015; Nunez et al., 2016;

Wright et al., 2015).

Bacteriophages can use naturally occurring anti-CRISPR proteins (Acrs) to antagonize the CRISPR-Cas immunity in bacteria (Bondy-Denomy et al., 2019; Bondy-Denomy et al., 2013). A number of Acrs have been identified for type I (Bondy-Denomy et al., 2013; He et al., 2018; Marino et al., 2018; Pawluk et al., 2014; Pawluk et al., 2016b), type II (Hynes et al., 2017; Pawluk et al., 2016a; Rauch et al., 2017; Uribe et al., 2019) and type V (Marino et al., 2018; Watters et al., 2018) CRISPR-Cas systems. These naturally occurring off-switches can be exploited to tune the activity and specificity of CRISPR-Cas9 activity in human cells (Harrington et al., 2017; Hynes et al., 2018; Pawluk et al., 2016a; Rauch et al., 2017; Shin et al., 2017). Currently known Acrs inhibit CRISPR-Cas systems by interfering with Cas protein-mediated DNA surveillance or cleavage (Pawluk et al., 2018). For instance, AcrIIA4 mimics double-stranded DNA (dsDNA) and occupies the protospacer adjacent motif (PAM) recognition site of SpyCas9, thereby preventing Cas9 protein from binding to the target DNA (Dong et al., 2017; Shin et al., 2017; Yang and Patel, 2017). Using a different mechanism, AcrIIC3 perturbs DNA binding by inducing the dimerization of Cas9 protein (Harrington et al., 2017). An alternative Cas inactivation strategy by Acrs is to interact with DNA-bound Cas proteins and block subsequent DNA cleavage, as seen with AcrF3 (Wang et al., 2016a; Wang et al., 2016b) and AcrIIC1 (Harrington et al., 2017). In addition, some Acrs can function as acetyltransferase and inactivate CRISPR-Cas activity by post-translational modifications (Dong et al., 2019). Different Acrs may inactivate CRISPR-Cas via identical mechanisms while possessing low sequence

similarities (Pawluk et al., 2018). The Acrs characterized to date share no common sequence motifs except for a putative transcriptional element referred to as anti-CRISPR associated genes (Acas) that are commonly found downstream of the Acr genes in the bacteriophage genome (Pawluk et al., 2016b).

Acrs can be adapted to inhibit CRISPR-Cas activities in bacteria (Lee et al., 2018), yeast (Basgall et al., 2018) and mammalian cells (Lee et al., 2018). Biosensor (Li et al., 2018c) and synthetic circuits (Nakamura et al., 2019) can be devised based on CRISPR-Cas coupled with Acrs. Moreover, Acrs can be harnessed to enable the temperature-responsive (Jiang et al., 2019) and optogenetic (Bubeck et al., 2018) control of CRISPR-Cas activity. Importantly, Acrs can enhance the editing (Shin et al., 2017) and cell-type (Hoffmann et al., 2019) specificities and reduce the cytotoxicity (Li et al., 2018b) of CRISPR-Cas-mediated genome editing. Acrs can be also employed to facilitate the production of CRISPR-carrying viral vectors by restricting CRISPR self-cleavage (Palmer et al., 2019).

Despite the advantages, most Acrs are 10-25 kDa in size and impermeable to mammalian cells (Maji et al., 2019). Although cell-permeable small-molecule Cas inhibitors have been reported, relative high concentrations of 10 μM or above are required for efficient inhibition. Along with the small molecule and protein-based Cas inhibitors, peptides represent an alternative class of Cas-inhibiting agents with distinct biochemical features. In this study, we report the unexpected discovery of Cas-inactivating peptides derived from inoviridae bacteriophages. In an attempt to develop anti-CRISPR antibodies using well established phage display technology, we are

surprised to discover that the commonly used laboratory bacteriophage strain M13 can serve as a source of Cas-inhibiting agent. Subsequent analyses showed that the periplasmic domain of the major coat protein G8P ($G8P_{PD}$) from inoviridae bacteriophages, which contain M13 phage, can inhibit the *in vitro* and *in vivo* activity of SpyCas9 in an allosteric manner. Most importantly, timed delivery of $G8P_{PD}$ can reduce the off-target activity of SpyCas9 with minimum interruption of its on-target activity. Our study hence expands the Cas inhibitor toolbox for precision genome editing.

RESULTS

Intact M13 Phage Inhibits the *In Vitro* DNA Cleavage Activity of SpyCas9

In a conventional phage display experiment, we surprisingly discovered that intact M13 phage (Smith and Petrenko, 1997) itself could efficiently block the DNA cleavage activity of purified SpyCas9 proteins (Figure 1A). Interestingly, phage-mediated SpyCas9 inactivation occurred only if phage was supplemented to the reaction prior to the addition of sgRNA (Figure 1A), but not post the formation of SpyCas9-sgRNA ribonucleoproteins (RNPs) (Figure 1B). M13 phage inhibited SpyCas9 activity in dose-dependent manner with an approximate half maximum inhibitory concentration (IC_{50}) of 5 nM (Figure 1C), which corresponds to a phage titer of 3×10^9 PFU/μL. The order-of-addition-dependent inhibition suggested that competition for sgRNA-binding site in SpyCas9 is a possible mechanism of the inhibitory activity of M13 phage.

M13 Phage Major Coat Protein-derived Peptide Inhibits the *In Vitro* DNA Cleavage Activity of SpyCas9

Next we sought to determine the components in M13 phage that contribute to SpyCas9 inactivation. M13 phage has a simple, compact genome comprising of 11 protein-coding sequences. Considering the accessibility, surface-exposed phage proteins most likely serve as the sources of Cas9-inhibiting agents. Fully packaged M13 phage contains approximately 2700 copies of major coat protein pVIII (G8P) and 5 copies each of minor coat proteins pIII, pVI, pVII and pXI (Marvin, 1998; Morag et al., 2015; van Wezenbeek et al., 1980). We initiated our investigation on the major coat protein G8P due to its abundance on M13 phage surface. The 73-amino acid major coat protein G8P contains four segments including signal peptide, periplasmic domain, transmembrane helix and cytoplasmic domain (Figure 1D). After G8P maturation, signal peptide is cleaved and transmembrane helix is inserted into phage membrane, leaving periplasmic domain the only region on phage surface. Therefore, we synthesized a 21-amino acid peptide constituting the periplasmic domain of G8P ($G8P_{PD}$) and examined its inhibitory activity on SpyCas9.

Similar to the intact phage, $G8P_{PD}$ suppressed the *in vitro* DNA cleavage of SpyCas9 in an order-of-addition-dependent manner (Figure 1D and F), indicating that $G8P_{PD}$ may inactivate SpyCas9 by specifically interfering with apo-SpyCas9. It was also noted that $G8P_{PD}$ inhibited the activity of SpyCas9 with an IC_{50} of 5 μM, which was 1000-fold lower than that of intact M13 phage.

In an effort to Blast search peptide homologs of M13 $G8P_{PD}$, we identified $G8P_{PD}$

from f1 phage which has only one amino acid difference from M13 $G8P_{PD}$ (Figure S1A). Because M13 and f1 $G8P_{PD}$ peptides have similar amino acid sequences and Cas9-inhibiting activities (Figure S1B), they were used interchangeably in the following studies.

$G8P_{PD}$ Prevents the Assembly of Cas9 and sgRNA by Binding to apo-Cas9

SpyCas9 can be inactivated at distinct steps during its action including guide RNA binding, substrate DNA binding and DNA cleavage. Most previously known Acrs exert their inhibitory activity by interfering with DNA surveillance or cleavage. To understand the mechanism of actions of $G8P_{PD}$, we examined the interactions between $G8P_{PD}$ and apo-Cas9 or Cas9-sgRNA RNP using electrophoresis mobility shift assay (EMSA). In the absence of $G8P_{PD}$, the fraction of Cas9-bound sgRNA increased with the increasing molar ratio of Cas9 and sgRNA with sgRNA concentration fixed to 15 μM. By contrast, pre-incubation of SpyCas9 proteins with 300 μM f1 $G8P_{PD}$ markedly reduced the fraction of Cas9-bound sgRNA under the same Cas9-sgRNA molar ratio (Figure 2A). We also noticed that under high molar ratio of Cas9 and sgRNA, 300 μM $G8P_{PD}$ did not fully block the formation of Cas9-sgRNA RNP (Figure 2A), suggesting a weak interaction between Cas9 and $G8P_{PD}$. Consistent with $G8P_{PD}$-medited inhibition of Cas9 cleavage, $G8P_{PD}$ prevented Cas9-sgRNA assembly in a dose-dependent manner (Figure 2B).

$G8P_{PD}$-mediated inhibition of Cas9-sgRNA assembly is dependent on the order of sgRNA addition. Under a fixed Cas9-sgRNA molar ratio of 0.5, pre-incubation of Cas9

with 300 or 600 μM f1 $G8P_{PD}$ prior to sgRNA addition abolished the assembly of Cas9 and sgRNA (Figure 2C). By contrast, supplementation of 300 or 600 μM $G8P_{PD}$ post sgRNA addition did not prevent the formation of Cas9-sgRNA complex (Figure 2D). These results suggest that $G8P_{PD}$ prevents Cas9-sgRNA binding by interacting with apo-Cas9 but not sgRNA-bound Cas9 and may explain why $G8P_{PD}$-mediated inactivation of SpyCas9 cleavage is dependent on the order of sgRNA addition.

Identification of $G8P_{PD}$ Binding Site in SpyCas9

In order to dissect the mechanism of interactions between SpyCas9 and $G8P_{PD}$, we sought to determine the binding region of $G8P_{PD}$ on SpyCas9 using high-resolution mass spectrometry (MS). SpyCas9 protein and M13 $G8P_{PD}$ were crosslinked using collision-induced dissociation (CID)-cleavable cross-linker disuccinimido sulfoxide (DSSO) (Kao et al., 2011) and then were subject to digestion with chymotrypsin. The integration analyses of CID-induced cleavage of interlinked peptides in MS/MS and MS^3 of single peptide chain fragment ions revealed high crosslinking scores (Figure 3A) on residues K1158 of [K]SVKEL peptide and K1176 of E[K]NPIDFLEAKGY peptide from SpyCas9 (Figure 3B-C and Figure S2A-B). These peptides occupy a continuous region in the PAM-interacting (PI) domain of SpyCas9 (Figure 3D) that is responsible for recognizing the PAM sequence on the non-complementary DNA strand (Nishimasu et al., 2014). Interestingly, this candidate $G8P_{PD}$ binding site dose not locate in the sgRNA or DNA binding pockets of SpyCas9. These results suggest that $G8P_{PD}$ does not directly compete with sgRNA but may instead function as an allosteric

inhibitor.

Next we sought to perform mutational analyses on the candidate $G8P_{PD}$ binding sites in SpyCas9. Residues KSKVEL in K1158 mutant and EKNPID in K1176 mutant were mutated into alanines respectively and the mutant SpyCas9 proteins were purified into high homogeneity (Figure S3A-B). *In vitro* cleavage reaction illustrated that alanine mutations at positions KSKVEL (K1158 mutant) and EKNPID (K1176 mutant) markedly reduced the DNA cleavage activity of SpyCas9 (Figure 3E), suggesting the importance of the $G8P_{PD}$ binding sites for SpyCas9 activity.

α-helical Structure is Critical for the Inhibitory Activity of $G8P_{PD}$

Next we performed an alanine scan on f1 phage $G8P_{PD}$ to illustrate its structural determinants for Cas9 inhibition. Four peptide mutants are designed with alanine mutations spanning the entire $G8P_{PD}$ sequence (Figure 4A). Alanine mutations at positions 6 to 11 abolished the inhibitory activity of $G8P_{PD}$ while mutants 1, 3 and 4 retained the majority of Cas9-inhibiting activity (Figure 4A). The major coat protein G8P adopts an α-helical structure (Morag et al., 2015). Residues 6 to 11 are located at the N-terminus of the α helix and contain Pro6, Lys8, Phe11 and three native alanines (Figure 4B). The abolished activity in mutant 2 suggested a critical role of positions 6 to 11, particularly the residues Pro6, Lys8 and Phe11. Circular dichroism (CD) spectra study revealed an α-helical structure-enriched feature for f1 $G8P_{PD}$ WT but not for mutant 2 (Figure 4C), suggesting that Pro6, Lys8 and Phe11 are important for maintaining the α-helical structure in f1 $G8P_{PD}$. Although the presence of residues 6 to

11 could directly participate in the interaction between Cas9 and $G8P_{PD}$, the overall α-helical structure of $G8P_{PD}$ could be also important for its Cas9-inhibiting activity.

Modulation of SpyCas9 Activity in Human Cells Using Inoviradae Phage $G8P_{PD}$

Encouraged by the *in vitro* inhibitory activity of $G8P_{PD}$, we next explored the potential application of $G8P_{PD}$ as an off-switch for the genome-editing activity of SpyCas9 in human cells. Ectopic expression of the full-length ($G8P_{FL}$) and periplasmic domain ($G8P_{PD}$) of M13 and f1 G8P at 24 h prior to Cas9-sgRNA transfection significantly suppressed the genome-editing activity of SpyCas9 in HEK293 cells (Figure 5A). In comparison, Acr protein AcrII4A (Shin et al., 2017) blocked SpyCas9 cleavage on *AAVS1* site whereas *Neisseria meningitidis* Cas9 (NmeCas9)-specific Acr protein AcrIIC3 (Zhu et al., 2019) partially inhibited SpyCas9. Importantly, f1 $G8P_{PD}$ was capable to inhibit SpyCas9 activity across different genes and cell types (Figure 5B). Consistent with the *in vitro* experiments, significant inhibition of the on-target activity of SpyCas9 in human cells was observed only when $G8P_{PD}$ was overexpressed prior to sgRNA transfection. Co-transfection of $G8P_{PD}$ and SpyCas9-sgRNA did not inhibit SpyCas9 cleavage ($P>0.05$) (Figure 5C).

In order to have detailed understanding of the effects of $G8P_{PD}$ on the genome-editing activity of SpyCas9, we performed next-generation sequencing to analyze the profiles of gene-edited genomic loci in the absence and presence of $G8P_{PD}$. Despite reduced mutation rate, the mutation pattern of SpyCas9 along the 20 bp sgRNA-targeting site was not altered by $G8P_{PD}$, as characterized by the high-frequency editing

events at 3 bp upstream of the PAM sequence (Jinek et al., 2012) (Figure 5D). Importantly, $G8P_{PD}$ treatment retained the distribution pattern of indel length, with 1-5 bp indel being predominant in the population (Figure S4A). In addition, we observed modest decrease in the in-frame mutations (3N) (Figure S4B), the mechanism of which is yet to be elucidated. Collectively, these data suggested that $G8P_{PD}$ treatment did not cause major alterations in the profiles of SpyCas9-induced mutations, thus highlighting the potential of $G8P_{PD}$ as SpyCas9 off-switch for therapeutic applications.

To extend peptide-based anti-CRISPR toolbox, we examined the G8Ps from other inoviridae phages (Figure S5). Peptides constituting the periplasmic domain of these G8P ($G8P_{PD}$) are synthesized and evaluated for the *in vitro* and *in vivo* activities. At a concentration of 10 μM, the $G8P_{PD}$ from M13, f1, Pf1 and I2-2 phage abolished the *in vitro* DNA cleavage activity of SpyCas9 while other $G8P_{PD}$ orthologs showed little inhibitory effects (Figure 5E). Ectopic expression of M13, f1 and M7 $G8P_{PD}$ in K562 cells significantly reduced the activity of SpyCas9 in HEK293 cells whereas $G8P_{PD}$ mutant 2 did not show inhibitory activity (P>0.05) (Figure 5F). Our results suggested that inoviridae phage G8Ps could be leveraged to inhibit both the *in vitro* and *in vivo* activity of SpyCas9. The variations of $G8P_{PD}$ sequences and the difference in their inhibitory activities indicate that further engineering endeavors could be made to improve Cas9-inhibiting peptides.

Timed Delivery of G8P Improves the Specificity of SpyCas9 in Human Cells

It has been reported that timed delivery of AcrIIA4 can improve the genome-editing

specificity of nucleofected Cas9-sgRNA RNP complex (Shin et al., 2017). We intended to investigate the effects of G8P peptides on the specificity of constitutively expressed SpyCas9, a more therapeutically relevant model. The aforementioned *in vitro* and *in vivo* data have suggested that the inhibitory effects of G8P on CRISPR-Cas9 is dependent on the accessibility of Cas9 protein to sgRNA. This observation prompted us to explore whether G8P can be leveraged, via timed delivery, to improve the specificity of SpyCas9. Unlike the above experiments using G8Ps as CRISPR off switch (Figure 5), in this experiment we co-transfected Hela cells with Acr or G8P plasmids and sgRNA and SpyCas9-coding plasmids. AcrIIA4 suppressed the on- and off-activities of SpyCas9 to undetectable levels, as determined by T7E1 assay (Figure 6A). Next-generation sequencing analyses of edited Hela cells showed that M13 $G8P_{FL}$ and f1 $G8P_{FL}$ significantly reduced ($P<0.05$) both the on-target and off-target activity of SpyCas9 though the inhibitory effects on the off-target site appeared to be more prominent (Figure 6B). AcrIIC3 significantly reduced the on-target activity ($P<0.05$) but not the off-target activity ($P>0.05$) (Figure 6B). Importantly, M13 $G8P_{PD}$ could reduce the off-target events without affecting the on-target cleavage (Figure 6B). Similarly, M13 $G8P_{PD}$ reduced the off-target events of SpyCas9 in K562 cells but retained the on-target activity (Figure 6C). Co-transfection of M13 $G8P_{FL}$ or f1 $G8P_{FL}$ in K562 cells led to minimum or no significant decrease in the on-target activity of SpyCas9 but markedly reduced the off-target events (Figure 6C). Surprisingly, AcrIIC3 did not significantly interrupt the on-target activity of SpyCas9 but notably increase the off-target activity (Figure 6C). Collectively, these data suggest that timed delivery of

$G8P_{PD}$-based anti-CRISPR agents (Figure 6D) can reduce the off-target events of constitutively expressed SpyCas9 in human cells without perturbing its on-target activity.

DISCUSSION

In this study, we reported the unexpected discovery of anti-CRISPR peptides from inoviridae bacteriophages. The clue leading to this discovery was based on the observation that intact M13 phage inhibited the DNA cleavage activity of SpyCas9 in *in vitro* reactions. Although we focused the investigation on the major coat protein G8P in the present study, it is likely that other surface-exposed minor coat proteins may attribute to intact phage-mediated SpyCas9 inhibition.

Unlike previously described Acrs that inhibit CRISPR-Cas by disrupting DNA binding (Bondy-Denomy et al., 2015; Dong et al., 2017; Harrington et al., 2017) or DNA cleavage (Harrington et al., 2017), G8P inactivates CRISPR-Cas9 by preventing Cas9 from sgRNA binding. This represents a distinct mechanism for CRISPR-Cas inactivation and may have important implications for designing novel Cas9 off-switches. Moreover, both *in vitro* and *in vivo* studies showed that to achieve efficient inhibition, $G8P_{PD}$ must access SpyCas9 prior to its binding with sgRNA, indicating that $G8P_{PD}$ binds to apo-Cas9, but not sgRNA-bound Cas9. These results suggest that $G8P_{PD}$ and sgRNA are mutually exclusive for binding with Cas9 nuclease. One straightforward explanation is that $G8P_{PD}$ and sgRNA compete for the same binding pocket. However, MS and mutational studies suggest that the binding site of f1 $G8P_{PD}$ is located on the PI domain of Cas9, distal from sgRNA or DNA binding pockets, thus suggesting against direct competition between $G8P_{PD}$ and sgRNA. It is known that the binding of guide RNA can induce conformational rearrangements of Cas9 (Jinek et al., 2014). It is possible that upon $G8P_{PD}$ or sgRNA binding SpyCas9 can transform from a flexible

conformation to a closed conformation, which prevents SpyCas9 from binding with the other counterpart. This allosteric inhibition mode are seen with small-molecule Cas inhibitors (Maji et al., 2019) and may have important implications for developing next-generation anti-CRISPR agents.

Existing Acr proteins can display nanomolar binding affinity to Cas9 (Harrington et al., 2017). In contrast, inoviridae phage $G8P_{PD}$ peptides exhibit weak affinity as evidenced by the micromolar IC_{50} in the *in vitro* cleavage reaction (Figure 1) and by its inability to completely block the assembly of Cas9-sgRNA RNP (Figure 2). Interestingly, intact M13 phage inhibits Cas9 with an IC_{50} of approximately 5 nM, 1000-fold lower than that with $G8P_{PD}$. The increased inhibitory activity with intact phage may result from the enhanced cooperativity and avidity afforded by the multimeric assembly of the phage capsid that carries 2700 copies of G8P.

Although we have demonstrated that inoviridae phage $G8P_{PD}$ can function as anti-CRISPR peptides, the biological relevance of our discovery is yet to be explored. Under native context, the major coat protein G8P does not enter bacterial cytoplasm during phage infection. It is thus unlikely for G8P to exert anti-CRISPR function at the early stage of phage infection. Instead, G8P could interact with CRISPR-Cas in bacterial cytoplasm after the phage genome is translated. This post-translational inhibitory activity will require G8P-coding DNA to evade CRISPR attack during phage infection. Further *in vivo* studies are needed to reveal the biological function of G8P under native context. In addition, the SpyCas9-inactivating $G8P_{PD}$ discovered in the present study are encoded by phages that infect *Escherichia coli* and *Pseudomonas aeruginosa*,

which do not harbor type II CRISPR-Cas system. Horizontal gene transfer could explain for the cross-species CRISPR inactivation (Pawluk et al., 2016b; Uribe et al., 2019), however a systemic phylogenetic analysis is necessary to reveal the evolutionary implications of the anti-CRISPR activity of G8Ps.

Despite the elusive biological relevance of the anti-CRISPR activity of G8P, we nevertheless demonstrated that the genome-editing activity of SpyCas9 in human cells can be modulated by $G8P_{PD}$. To the best of our knowledge, our discovery represents the first peptides known to exhibit Cas9-inhibiting activity and expands the anti-CRISPR agent toolbox which is currently composed of Cas-inactivating proteins (Pawluk et al., 2018), small-molecules (Maji et al., 2019) and synthetic oligonucleotides (Li et al., 2018a). Compared with Acr proteins that are typically 10 to 20 kD in size, $G8P_{PD}$ peptides are small in size and can be chemically synthesized in large scale using solid phase synthesis or equivalent technologies. The facile manufacturing process is critical for the rapid evaluation of the structure-activity relationship to identify enhanced anti-CRISPR peptides, particularly given that our analyses of different inoviridae phage $G8P_{PD}$ supports the notion of improving SpyCas9-inhibiting peptides by engineering endeavors.

$G8P_{PD}$ does not alter the pattern of SpyCas9-induced mutations, suggesting that $G8P_{PD}$-mediated Cas9 inactivation does not interfere with the downstream DNA repair pathway. This feature facilitates the therapeutic applications of $G8P_{PD}$ as CRISPR off-switches by restricting the alterations of genome-editing outcome. It has been shown that AcrIIA4 can improve the specificity of Cas9 RNP-mediated genome editing (Shin

et al., 2017). However, most current CRISPR-Cas delivery systems in clinical applications involve constitutively active SpyCas9. Our study report for the first time that anti-CRISPR peptides can be leveraged to improve the specificity of constitutively expressed SpyCas9, thus providing insight into the potential application of anti-CRISPR agents under therapeutically relevant context.

It has been proposed that the specificity of SpyCas9 in human cells may be increased by partial inhibition with weak CRISPR inhibitors (Maji et al., 2019). In the current study, we found that timed delivery of strong CRISPR inhibitor AcrII4A prior to (Figure 5A) and simultaneously with (Figure 6A) sgRNA- and SpyCas9-coding plasmids in human cells displayed near complete inhibition of both on-target and off-target activities of SpyCas9. By contrast, co-delivery of G8P with CRISPR-Cas9 showed little inhibition of the on-target activity but reduced the off-target events. Thus, our results proved the concept for the first time that weak CRISPR inhibitors can be adapted to improve the genome-editing specificity of constitutively expressed nucleases.

Interestingly, it was observed that the AcrIIC3, a weak inhibitor to SpyCas9 (Figure 5A), did not increase the specificity of SpyCas9 in human cells (Figure 6B-C). This result along with the results of $G8P_{PD}$ suggest that the mechanism of actions of the inhibitors may be also important for their effects on the specificity of CRISPR-Cas9. Unlike previous known protein- or small molecule-based inhibitors, $G8P_{PD}$ interfere with SpyCas9-sgRNA assembly in an allosteric manner, a unique mechanism among CRISPR inhibitors. The SpyCas9-inhibiting activity of $G8P_{PD}$ is suppressed by the complexation of SpyCas9 with sgRNA, presumably due to the structural constraints

introduced by sgRNA binding. Because SpyCas9 has high affinity to sgRNA (Jinek et al., 2012) but low affinity to $G8P_{PD}$ (Figure 2), co-delivery of $G8P_{PD}$- and sgRNA-coding genes with SpyCas9 plasmid will lead to predominating Cas9-sgRNA complex at the early stage. The newly synthesized Cas9 protein will be occupied by saturating $G8P_{PD}$ at subsequent stage. This two-stage action mode (Figure 6D) thus allows for the reduction of off-target events associated with prolonged Cas9 expression while having little impact on the on-target activity. This unique mechanism of G8P may also provide insights into designing anti-CRISPR agents towards other genome- or base-editing systems.

In summary, we describe in the present study phage-derived peptides that inhibit the *in vitro* and *in vivo* activities of SpyCas9 and show that these peptides can be harnessed to improve the specificity of constitutively expressed SpyCas9 for precision genome editing.

STAR METHODS

Detailed methods are provided in the online version of this paper and include the following:

- KEY RESOURCES TABLE
- CONTACT FOR REAGENT AND RESOURCE SHARING
- EXPERIMENTAL MODEL AND SUJECT DETAILS
  - *Escherichia coli* (XL1-Blue)
  - *E. coli* (BL21)
  - M13 bacteriophage
  - Cell Culture
- METHOD DETAILS
  - Expression and purification of SpyCas9 protein
  - Construction of $G8P_{PD}$ overexpression plasmids
  - *In vitro* transcription of sgRNA
  - *In vitro* cleavage assay
  - Electrophoresis mobility shift assay (EMSA)
  - Chemical crosslinking and mass spectrometry
  - Circular dichroism
  - Inhibition of CRISPR-Cas9 activity in human cells by $G8P_{PD}$ overexpression
  - Next-generation sequencing of edited genomic sites
- QUANTIFICATION AND STATISTICAL ANALYSES
- DATA AND SOFTWARE AVAILABILITY

SUPPLEMENTAL INFORMATION

Supplemental Information can be found online.

ACKNOWLEDGEMENTS

This work is supported by the National Natural Science Foundation of China (31600686 to J.L. and 31500632 to P.M.) and ShanghaiTech University Startup Fund (2019F0301-000-01 to J.L.). We thank the Analytical Platform and High-Throughput Screening Platform at Shanghai Institute for Advanced Immunochemical Studies (SIAIS) at ShanghaiTech University for the support of mass spectrometry and flow cytometry experiments.

AUTHOR CONTRIBUTIONS

P.M. and J.L. conceptualized study. P.M., J.L., Y.-R.C. and S.-J.W. designed the experiments and analyzed data. Y.-R.C. and S.-J.W. performed the *in vitro* and *in vivo* Cas9-inhibiting experiments. J.C. analyzed next-generation sequencing data. J.Li manufactured M13 phage and initial phage selections. P.M. and S.W performed the crosslink experimenting. W.C. and W.Z. performed MS experiment and analyzed the data. B.M. and B.Y. provided purified WT SpyCas9 proteins and advice on the purification of other SpyCas9 variants. S.W. and Z.Z. helped to express and purify SpyCas9 proteins. B.J. and G.Y. provided critical resources. P.M. and J.L. wrote the manuscript. All authors discussed the results and commented on and approved the

manuscript.

DECLARATION OF INTERESTS

J.L., B.J., P.M. and G.Y. has filed a patent application including the work described herein.

References

Barrangou, R., Fremaux, C., Deveau, H., Richards, M., Boyaval, P., Moineau, S., Romero, D.A., and Horvath, P. (2007). CRISPR provides acquired resistance against viruses in prokaryotes. Science *315*, 1709-1712.

Basgall, E.M., Goetting, S.C., Goeckel, M.E., Giersch, R.M., Roggenkamp, E., Schrock, M.N., Halloran, M., and Finnigan, G.C. (2018). Gene drive inhibition by the anti-CRISPR proteins AcrIIA2 and AcrIIA4 in Saccharomyces cerevisiae. Microbiology *164*, 464-474.

Bondy-Denomy, J., Davidson, A.R., Doudna, J.A., Fineran, P.C., Maxwell, K.L., Moineau, S., Peng, X., Sontheimer, E.J., and Wiedenheft, B. (2019). A unified resource for tracking anti-CRISPR names The CRISPR Journal *1*, 304-305.

Bondy-Denomy, J., Garcia, B., Strum, S., Du, M., Rollins, M.F., Hidalgo-Reyes, Y., Wiedenheft, B., Maxwell, K.L., and Davidson, A.R. (2015). Multiple mechanisms for CRISPR-Cas inhibition by anti-CRISPR proteins. Nature *526*, 136-139.

Bondy-Denomy, J., Pawluk, A., Maxwell, K.L., and Davidson, A.R. (2013). Bacteriophage genes that inactivate the CRISPR/Cas bacterial immune system. Nature *493*, 429-432.

Brouns, S.J., Jore, M.M., Lundgren, M., Westra, E.R., Slijkhuis, R.J., Snijders, A.P., Dickman, M.J., Makarova, K.S., Koonin, E.V., and van der Oost, J. (2008). Small CRISPR RNAs guide antiviral defense in prokaryotes. Science *321*, 960-964.

Bubeck, F., Hoffmann, M.D., Harteveld, Z., Aschenbrenner, S., Bietz, A., Waldhauer, M.C., Borner, K., Fakhiri, J., Schmelas, C., Dietz, L., *et al.* (2018). Engineered anti-CRISPR proteins for optogenetic control of CRISPR-Cas9. Nat Methods *15*, 924-927.

Cao, J., Wu, L., Zhang, S.M., Lu, M., Cheung, W.K., Cai, W., Gale, M., Xu, Q., and Yan, Q. (2016). An easy and efficient inducible CRISPR/Cas9 platform with improved specificity for multiple gene targeting. Nucleic Acids Res *44*, e149.

Cho, S.W., Kim, S., Kim, J.M., and Kim, J.S. (2013). Targeted genome engineering in human cells with the Cas9 RNA-guided endonuclease. Nat Biotechnol *31*, 230-232.

Cong, L., Ran, F.A., Cox, D., Lin, S., Barretto, R., Habib, N., Hsu, P.D., Wu, X., Jiang, W., Marraffini, L.A., *et al.* (2013). Multiplex genome engineering using CRISPR/Cas systems. Science *339*, 819-823.

Dong, Guo, M., Wang, S., Zhu, Y., Xiong, Z., Yang, J., Xu, Z., and Huang, Z. (2017). Structural basis of CRISPR-SpyCas9 inhibition by an anti-CRISPR protein. Nature *546*, 436-439.

Dong, L., Guan, X., Li, N., Zhang, F., Zhu, Y., Ren, K., Yu, L., Zhou, F., Han, Z., Gao,

N., *et al.* (2019). An anti-CRISPR protein disables type V Cas12a by acetylation. Nat Struct Mol Biol *26*, 308-314.

Fellmann, C., Gowen, B.G., Lin, P.C., Doudna, J.A., and Corn, J.E. (2017). Cornerstones of CRISPR-Cas in drug discovery and therapy. Nat Rev Drug Discov *16*, 89-100.

Fu, Y., Sander, J.D., Reyon, D., Cascio, V.M., and Joung, J.K. (2014). Improving CRISPR-Cas nuclease specificity using truncated guide RNAs. Nat Biotechnol *32*, 279-284.

Guschin, D.Y., Waite, A.J., Katibah, G.E., Miller, J.C., Holmes, M.C., and Rebar, E.J. (2010). A rapid and general assay for monitoring endogenous gene modification. Methods Mol Biol *649*, 247-256.

Harrington, L.B., Doxzen, K.W., Ma, E., Liu, J.J., Knott, G.J., Edraki, A., Garcia, B., Amrani, N., Chen, J.S., Cofsky, J.C., *et al.* (2017). A broad-spectrum inhibitor of CRISPR-Cas9. Cell *170*, 1224-1233 e1215.

He, F., Bhoobalan-Chitty, Y., Van, L.B., Kjeldsen, A.L., Dedola, M., Makarova, K.S., Koonin, E.V., Brodersen, D.E., and Peng, X. (2018). Anti-CRISPR proteins encoded by archaeal lytic viruses inhibit subtype I-D immunity. Nat Microbiol *3*, 461-469.

Hoffmann, M.D., Aschenbrenner, S., Grosse, S., Rapti, K., Domenger, C., Fakhiri, J., Mastel, M., Borner, K., Eils, R., Grimm, D., *et al.* (2019). Cell-specific CRISPR-Cas9 activation by microRNA-dependent expression of anti-CRISPR proteins. Nucleic Acids Res.

Hsu, P.D., Scott, D.A., Weinstein, J.A., Ran, F.A., Konermann, S., Agarwala, V., Li, Y., Fine, E.J., Wu, X., Shalem, O., *et al.* (2013). DNA targeting specificity of RNA-guided Cas9 nucleases. Nat Biotechnol *31*, 827-832.

Hynes, A.P., Rousseau, G.M., Agudelo, D., Goulet, A., Amigues, B., Loehr, J., Romero, D.A., Fremaux, C., Horvath, P., Doyon, Y., *et al.* (2018). Widespread anti-CRISPR proteins in virulent bacteriophages inhibit a range of Cas9 proteins. Nat Commun *9*, 2919.

Hynes, A.P., Rousseau, G.M., Lemay, M.L., Horvath, P., Romero, D.A., Fremaux, C., and Moineau, S. (2017). An anti-CRISPR from a virulent streptococcal phage inhibits Streptococcus pyogenes Cas9. Nat Microbiol *2*, 1374-1380.

Jiang, F., Liu, J.J., Osuna, B.A., Xu, M., Berry, J.D., Rauch, B.J., Nogales, E., Bondy-Denomy, J., and Doudna, J.A. (2019). Temperature-responsive competitive inhibition of CRISPR-Cas9. Mol Cell *73*, 601-610 e605.

Jinek, M., Chylinski, K., Fonfara, I., Hauer, M., Doudna, J.A., and Charpentier, E. (2012). A programmable dual-RNA-guided DNA endonuclease in adaptive bacterial

immunity. Science *337*, 816-821.

Jinek, M., East, A., Cheng, A., Lin, S., Ma, E., and Doudna, J. (2013). RNA-programmed genome editing in human cells. Elife *2*, e00471.

Jinek, M., Jiang, F., Taylor, D.W., Sternberg, S.H., Kaya, E., Ma, E., Anders, C., Hauer, M., Zhou, K., Lin, S., *et al.* (2014). Structures of Cas9 endonucleases reveal RNA-mediated conformational activation. Science *343*, 1247997.

Kao, A., Chiu, C.L., Vellucci, D., Yang, Y., Patel, V.R., Guan, S., Randall, A., Baldi, P., Rychnovsky, S.D., and Huang, L. (2011). Development of a novel cross-linking strategy for fast and accurate identification of cross-linked peptides of protein complexes. Mol Cell Proteomics *10*, M110 002212.

Koboldt, D.C., Zhang, Q., Larson, D.E., Shen, D., McLellan, M.D., Lin, L., Miller, C.A., Mardis, E.R., Ding, L., and Wilson, R.K. (2012). VarScan 2: somatic mutation and copy number alteration discovery in cancer by exome sequencing. Genome Res *22*, 568-576.

Koo, T., Lee, J., and Kim, J.S. (2015). Measuring and reducing off-target activities of programmable nucleases including CRISPR-Cas9. Mol Cells *38*, 475-481.

Kosicki, M., Tomberg, K., and Bradley, A. (2018). Repair of double-strand breaks induced by CRISPR-Cas9 leads to large deletions and complex rearrangements. Nat Biotechnol *36*, 765-771.

Langmead, B., and Salzberg, S.L. (2012). Fast gapped-read alignment with Bowtie 2. Nat Methods *9*, 357-359.

Lee, J., Mir, A., Edraki, A., Garcia, B., Amrani, N., Lou, H.E., Gainetdinov, I., Pawluk, A., Ibraheim, R., Gao, X.D., *et al.* (2018). Potent Cas9 inhibition in bacterial and human cells by AcrIIC4 and AcrIIC5 anti-CRISPR proteins. MBio *9*.

Li, B., Zeng, C., Li, W., Zhang, X., Luo, X., Zhao, W., Zhang, C., and Dong, Y. (2018a). Synthetic oligonucleotides inhibit CRISPR-Cpf1-mediated genome editing. Cell Rep *25*, 3262-3272 e3263.

Li, C., Psatha, N., Gil, S., Wang, H., Papayannopoulou, T., and Lieber, A. (2018b). HDAd5/35(++) adenovirus vector expressing anti-CRISPR peptides decreases CRISPR/Cas9 toxicity in human hematopoietic stem cells. Mol Ther Methods Clin Dev *9*, 390-401.

Li, H., and Durbin, R. (2009). Fast and accurate short read alignment with Burrows-Wheeler transform. Bioinformatics *25*, 1754-1760.

Li, H., Handsaker, B., Wysoker, A., Fennell, T., Ruan, J., Homer, N., Marth, G., Abecasis, G., and Durbin, R. (2009). The sequence alignment/map format and SAMtools. Bioinformatics *25*, 2078-2079.

Li, J., Xu, Z., Chupalov, A., and Marchisio, M.A. (2018c). Anti-CRISPR-based biosensors in the yeast *S. cerevisiae*. J Biol Eng *12*, 11.

Liu, F., Lossl, P., Scheltema, R., Viner, R., and Heck, A.J.R. (2017). Optimized fragmentation schemes and data analysis strategies for proteome-wide cross-link identification. Nat Commun *8*, 15473.

Maji, B., Gangopadhyay, S.A., Lee, M., Shi, M., Wu, P., Heler, R., Mok, B., Lim, D., Siriwardena, S.U., Paul, B., *et al.* (2019). A high-throughput platform to identify small-molecule inhibitors of CRISPR-Cas9. Cell *177*, 1067-1079.

Mali, P., Yang, L., Esvelt, K.M., Aach, J., Guell, M., DiCarlo, J.E., Norville, J.E., and Church, G.M. (2013). RNA-guided human genome engineering via Cas9. Science *339*, 823-826.

Marino, N.D., Zhang, J.Y., Borges, A.L., Sousa, A.A., Leon, L.M., Rauch, B.J., Walton, R.T., Berry, J.D., Joung, J.K., Kleinstiver, B.P., *et al.* (2018). Discovery of widespread type I and type V CRISPR-Cas inhibitors. Science *362*, 240-242.

Marraffini, L.A., and Sontheimer, E.J. (2008). CRISPR interference limits horizontal gene transfer in staphylococci by targeting DNA. Science *322*, 1843-1845.

Marvin, D.A. (1998). Filamentous phage structure, infection and assembly. Curr Opin Struct Biol *8*, 150-158.

Morag, O., Sgourakis, N.G., Baker, D., and Goldbourt, A. (2015). The NMR-Rosetta capsid model of M13 bacteriophage reveals a quadrupled hydrophobic packing epitope. Proc Natl Acad Sci U S A *112*, 971-976.

Nakamura, M., Srinivasan, P., Chavez, M., Carter, M.A., Dominguez, A.A., La Russa, M., Lau, M.B., Abbott, T.R., Xu, X., Zhao, D., *et al.* (2019). Anti-CRISPR-mediated control of gene editing and synthetic circuits in eukaryotic cells. Nat Commun *10*, 194.

Nihongaki, Y., Kawano, F., Nakajima, T., and Sato, M. (2015). Photoactivatable CRISPR-Cas9 for optogenetic genome editing. Nat Biotechnol *33*, 755-760.

Nishimasu, H., Ran, F.A., Hsu, P.D., Konermann, S., Shehata, S.I., Dohmae, N., Ishitani, R., Zhang, F., and Nureki, O. (2014). Crystal structure of Cas9 in complex with guide RNA and target DNA. Cell *156*, 935-949.

Nunez, J.K., Harrington, L.B., and Doudna, J.A. (2016). Chemical and biophysical modulation of Cas9 for tunable genome engineering. ACS Chem Biol *11*, 681-688.

Palmer, D.J., Turner, D.L., and Ng, P. (2019). Production of CRISPR/Cas9-mediated self-cleaving helper-dependent adenoviruses. Mol Ther Methods Clin Dev *13*, 432-439.

Pattanayak, V., Lin, S., Guilinger, J.P., Ma, E., Doudna, J.A., and Liu, D.R. (2013).

High-throughput profiling of off-target DNA cleavage reveals RNA-programmed Cas9 nuclease specificity. Nat Biotechnol *31*, 839-843.

Pawluk, A., Amrani, N., Zhang, Y., Garcia, B., Hidalgo-Reyes, Y., Lee, J., Edraki, A., Shah, M., Sontheimer, E.J., Maxwell, K.L., *et al.* (2016a). Naturallyoccurring off-switches for CRISPR-Cas9. Cell *167*, 1829-1838 e1829.

Pawluk, A., Bondy-Denomy, J., Cheung, V.H., Maxwell, K.L., and Davidson, A.R. (2014). A new group of phage anti-CRISPR genes inhibits the type I-E CRISPR-Cas system of Pseudomonas aeruginosa. MBio *5*, e00896.

Pawluk, A., Davidson, A.R., and Maxwell, K.L. (2018). Anti-CRISPR: discovery, mechanism and function. Nat Rev Microbiol *16*, 12-17.

Pawluk, A., Staals, R.H., Taylor, C., Watson, B.N., Saha, S., Fineran, P.C., Maxwell, K.L., and Davidson, A.R. (2016b). Inactivation of CRISPR-Cas systems by anti-CRISPR proteins in diverse bacterial species. Nat Microbiol *1*, 16085.

Rauch, B.J., Silvis, M.R., Hultquist, J.F., Waters, C.S., McGregor, M.J., Krogan, N.J., and Bondy-Denomy, J. (2017). Inhibition of CRISPR-Cas9 with bacteriophage proteins. Cell *168*, 150-158 e110.

Shin, J., Jiang, F., Liu, J.J., Bray, N.L., Rauch, B.J., Baik, S.H., Nogales, E., Bondy-Denomy, J., Corn, J.E., and Doudna, J.A. (2017). Disabling Cas9 by an anti-CRISPR DNA mimic. Sci Adv *3*, e1701620.

Smith, G.P., and Petrenko, V.A. (1997). Phage Display. Chem Rev *97*, 391-410.

Uribe, R.V., van der Helm, E., Misiakou, M.A., Lee, S.W., Kol, S., and Sommer, M.O.A. (2019). Discovery and characterization of Cas9 inhibitors disseminated across seven bacterial phyla. Cell Host Microbe *25*, 233-241 e235.

van Wezenbeek, P.M., Hulsebos, T.J., and Schoenmakers, J.G. (1980). Nucleotide sequence of the filamentous bacteriophage M13 DNA genome: comparison with phage fd. Gene *11*, 129-148.

Wang, J., Ma, J., Cheng, Z., Meng, X., You, L., Wang, M., Zhang, X., and Wang, Y. (2016a). A CRISPR evolutionary arms race: structural insights into viral anti-CRISPR/Cas responses. Cell Res *26*, 1165-1168.

Wang, X., Yao, D., Xu, J.G., Li, A.R., Xu, J., Fu, P., Zhou, Y., and Zhu, Y. (2016b). Structural basis of Cas3 inhibition by the bacteriophage protein AcrF3. Nat Struct Mol Biol *23*, 868-870.

Watters, K.E., Fellmann, C., Bai, H.B., Ren, S.M., and Doudna, J.A. (2018). Systematic discovery of natural CRISPR-Cas12a inhibitors. Science *362*, 236-239.

Wright, A.V., Sternberg, S.H., Taylor, D.W., Staahl, B.T., Bardales, J.A., Kornfeld, J.E., and Doudna, J.A. (2015). Rational design of a split-Cas9 enzyme complex. Proc Natl Acad Sci U S A *112*, 2984-2989.

Yang, H., and Patel, D.J. (2017). Inhibition Mechanism of an Anti-CRISPR Suppressor AcrIIA4 Targeting SpyCas9. Mol Cell *67*, 117-127 e115.

Zhu, Y., Gao, A., Zhan, Q., Wang, Y., Feng, H., Liu, S., Gao, G., Serganov, A., and Gao, P. (2019). Diverse mechanisms of CRISPR-Cas9 inhibition by type IIC anti-CRISPR proteins. Mol Cell *74*, 296-309 e297.

FIGURES AND LEGENDS

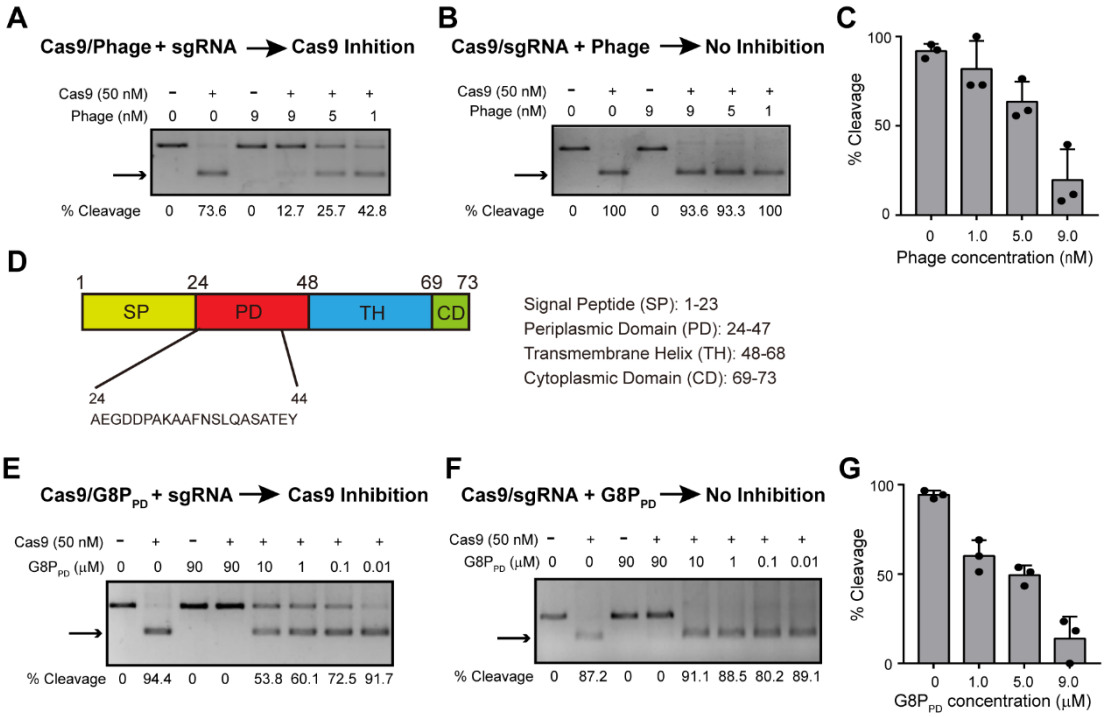

Figure 1. Inhibition of the *In Vitro* Activity of SpyCas9 by Intact M13 Phage and Phage-derived G8P$_{PD}$ Peptides. (A-B), Inhibition of the *in vitro* activity of SpyCas9 by intact M13 phage prior to (A) or post (B) the assembly of Cas9-sgRNA RNP. (C) Dose-dependent inhibition of SpyCas9 by intact M13 phage. (D) Structural organization of M13 phage major coat protein G8P. (E-F) Inhibition of the *in vitro* activity of SpyCas9 by G8P$_{PD}$ prior to (E) or post (F) the assembly of Cas9-sgRNA

RNP. **(G)** Dose-dependent inhibition of SpyCas9 by $G8P_{PD}$. The above reactions are performed in the absence or presence of 50 nM SpyCas9 proteins. The results are shown as mean ± SD (n = 3). Arrows indicate cleavage products.

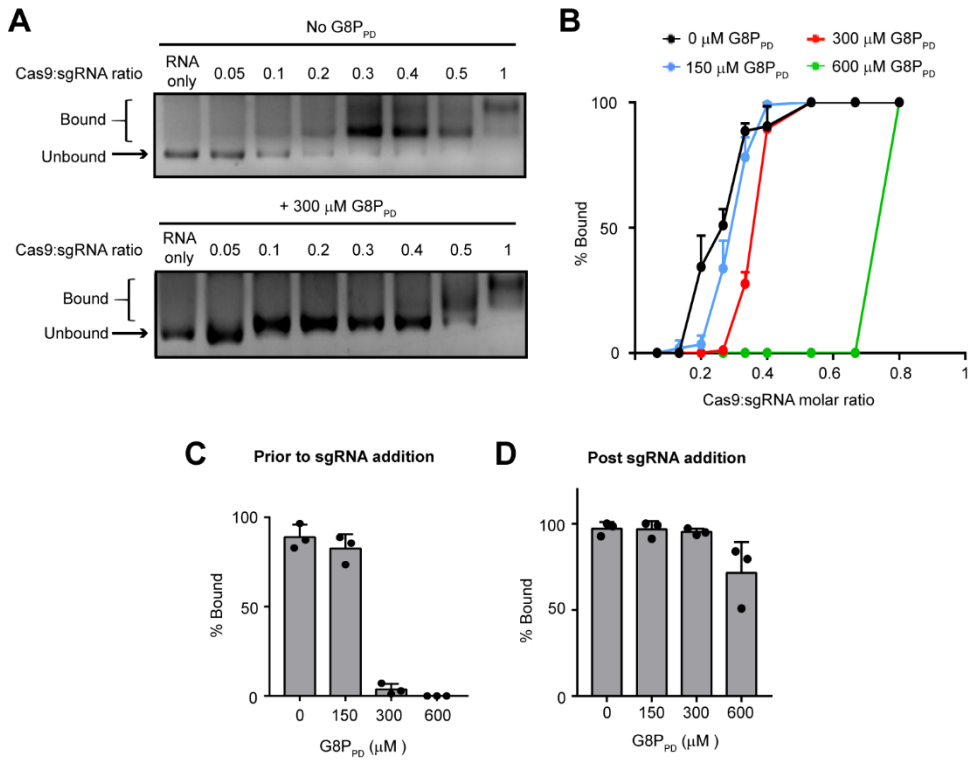

Figure 2. G8P$_{PD}$ Prevents Cas9-sgRNA Assembly. (A) f1 G8P$_{PD}$ disrupts the interaction between Cas9 and sgRNA, as determined by EMSA. Cas9-bound and unbound sgRNA are indicated. (B) Dose-dependent inhibition of Cas9-sgRNA binding by f1 G8P$_{PD}$. sgRNA concentration is fixed to 15 μM in (A-B). (C-D) f1 G8P$_{PD}$ prevents Cas9-sgRNA assembly prior to (C), but not post (D), sgRNA addition. Cas9 and sgRNA concentrations are fixed to 7.5 and 15 μM respectively in (C-D). The above results are shown as mean ± SD (n = 3).

A

Max. XlinkX Score	Seq. A	Acces. A	Pos. A	Seq. B	Acces. B	Pos. B	Crosslink	# CSMs	Protein. A	Protein. B
138.24	AEGDDPA[K]AAF	M13-pep	8	[K]SVKEL	Cas9	1158	DSSO; Inter	1	M13-pep	Cas9
102.5	E[K]NPIDFLEAKGY	Cas9	1176	AEGDDPA[K]AAF	M13-pep	8	DSSO; Inter	1	Cas9	M13-pep

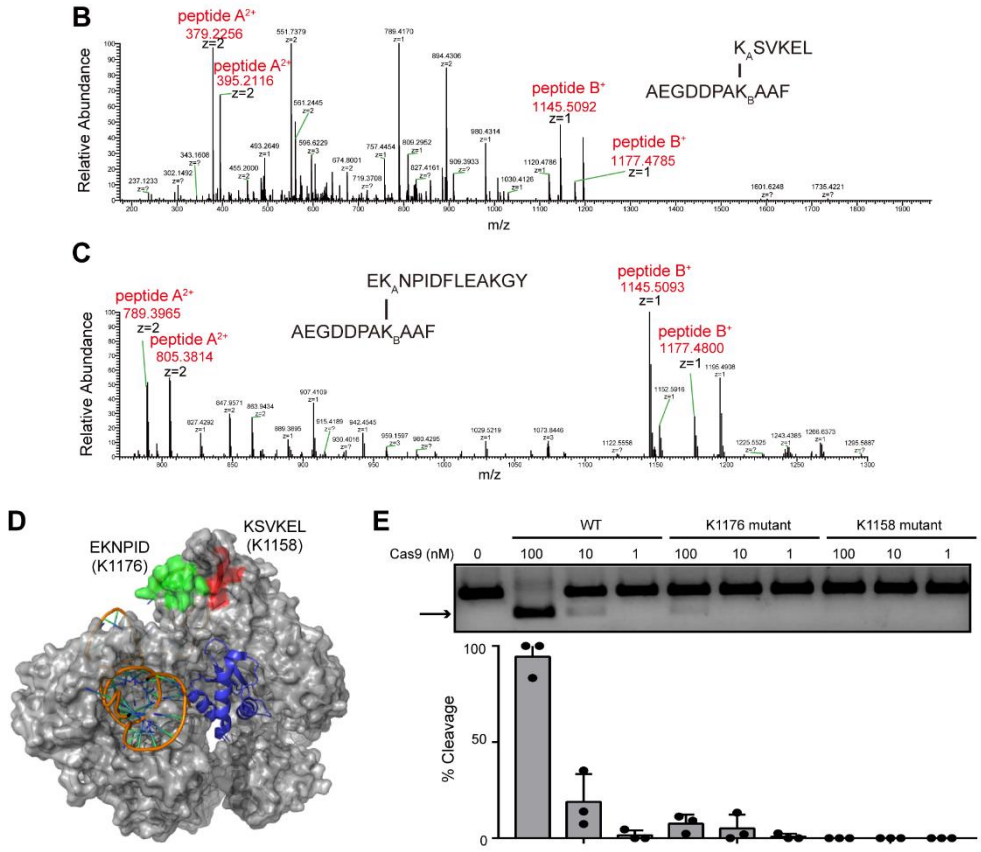

Figure 3. Identification of M13 G8P$_{PD}$ Binding Site in the PI domain of SpyCas9. (A) Maximum XlinkX scores of peptide hits in high-resolution MS analyses. (B) Secondary MS showing crosslinked peptides KSVKEL-AEGDDPAKAAF. (C) Secondary MS showing crosslinked peptides EKNPIDFLEAKGY-AEGDDPAKAAF. (D) Location of G8P$_{PD}$ binding sites in SpyCas9. The structure of SpyCas9 in complex with AcrIIA4 (5VW1) is displayed by PyMOL. AcrIIA4 is shown in blue. The candidate G8P$_{PD}$ binding sites on SpyCas9 are shown in green and red respectively. (E) *In vitro* DNA cleavage by WT, K1176 mutant and K1158 mutant SpyCas9. Arrow indicates cleavage product. The results are shown as mean ± SD (n = 3).

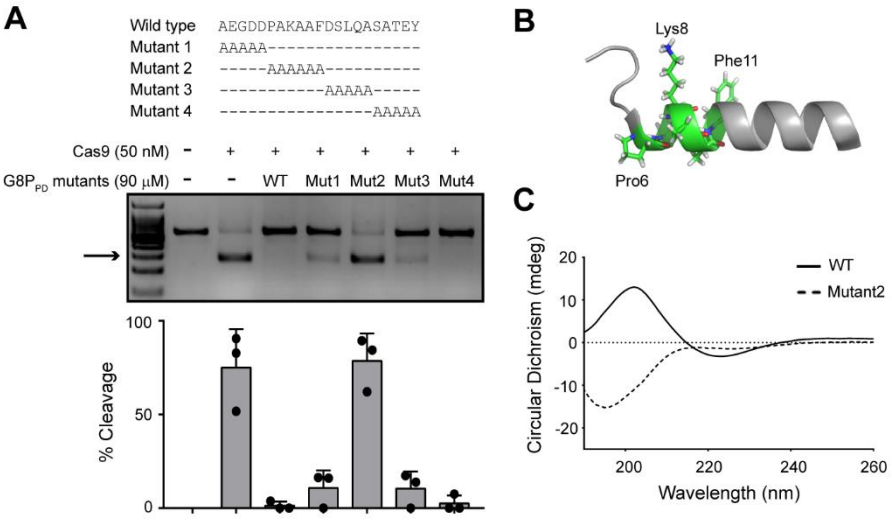

Figure 4. α-helical Structure is Critical for the Cas9-inhibiting Activity of G8P$_{PD}$. (A) Alanine mutations at position 6-11 abolish the inhibitory activity of G8P$_{PD}$. The results are shown as mean ± SD (n = 3). The arrow donates cleavage products. (B) Structure of G8P$_{PD}$ peptide (PDB entry 2MJZ), displayed by PyMOL. Residues 6-11 are shown as stick. (C) CD spectra of f1 G8P$_{PD}$ WT and mutant 2.

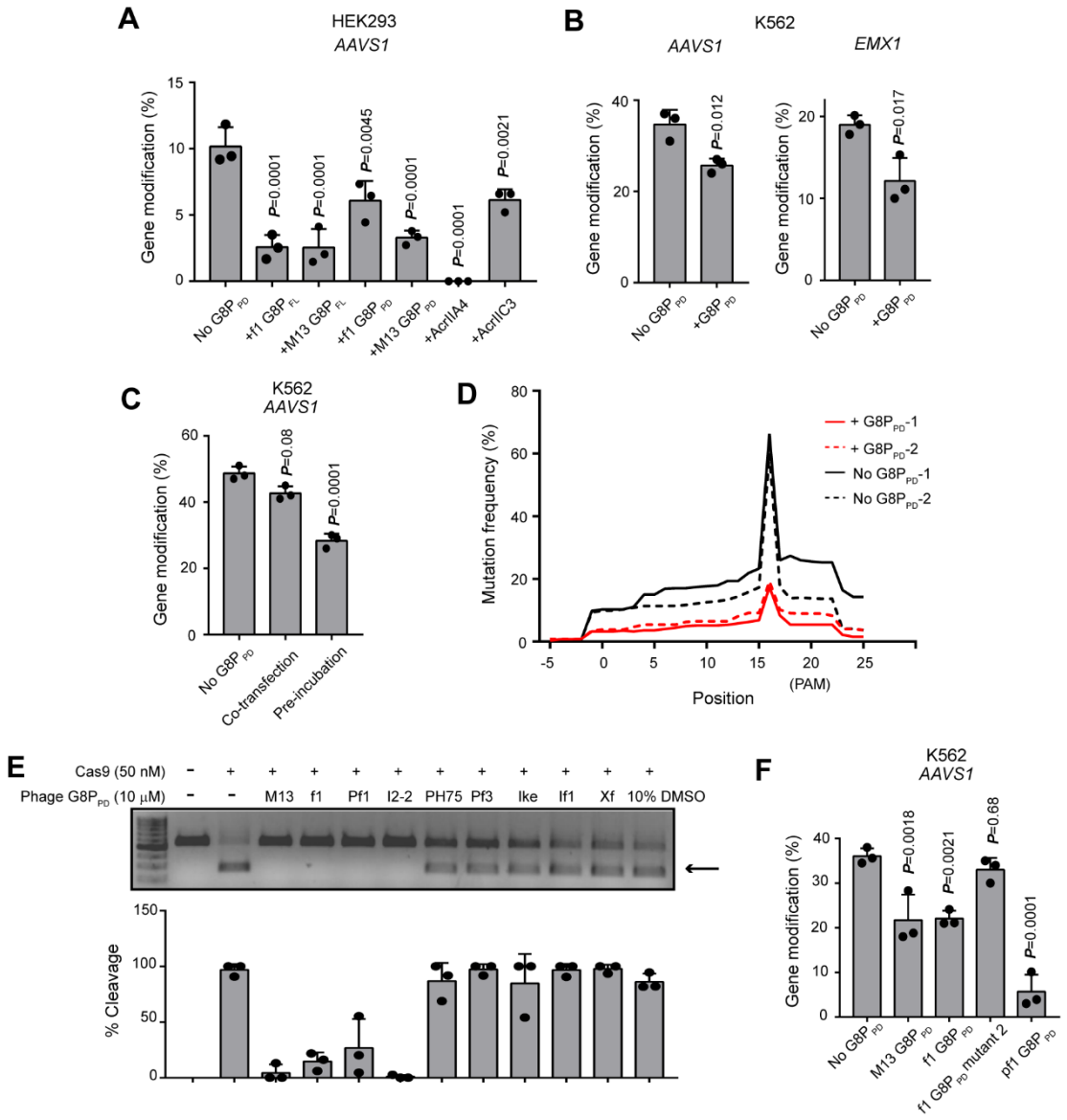

Figure 5. Inhibition of the Genome-editing Activity of SpyCas9 in Human Cells by Inoviridae PhageG8P$_{PD}$. (A) Comparison of SpyCas9-inhibiting activities of phage peptides and Acrs in HEK293 cells. (B) G8P$_{PD}$ inhibits the genome-editing activity of SpyCas9 across different genes and cell types. (C) The effects of G8P$_{PD}$ co-transfection and pre-incubation on the genome-editing activity of CRISPR-Cas9. (D) Density plot showing the next-generation sequencing analyses of the distribution of mutation rates along the gene-edited genomic sites of *AAVS1* in K562 cells. The results of two biological replicates are individually shown. (E) Inhibition of the *in vitro* DNA cleavage

activity of SpyCas9 by inoviridae $G8P_{PD}$. DMSO of 0.1% is included as a solvent control. Arrow donate cleavage products. (F) Inhibition of SpyCas9 activity in K562 cells by inoviridae $G8P_{PD}$. The results are shown as mean ± SD (n = 3). Significant difference between test groups and mock is determined by one-way ANOVA with Dunnett's multiple comparisons test. The adjusted P values are indicated.

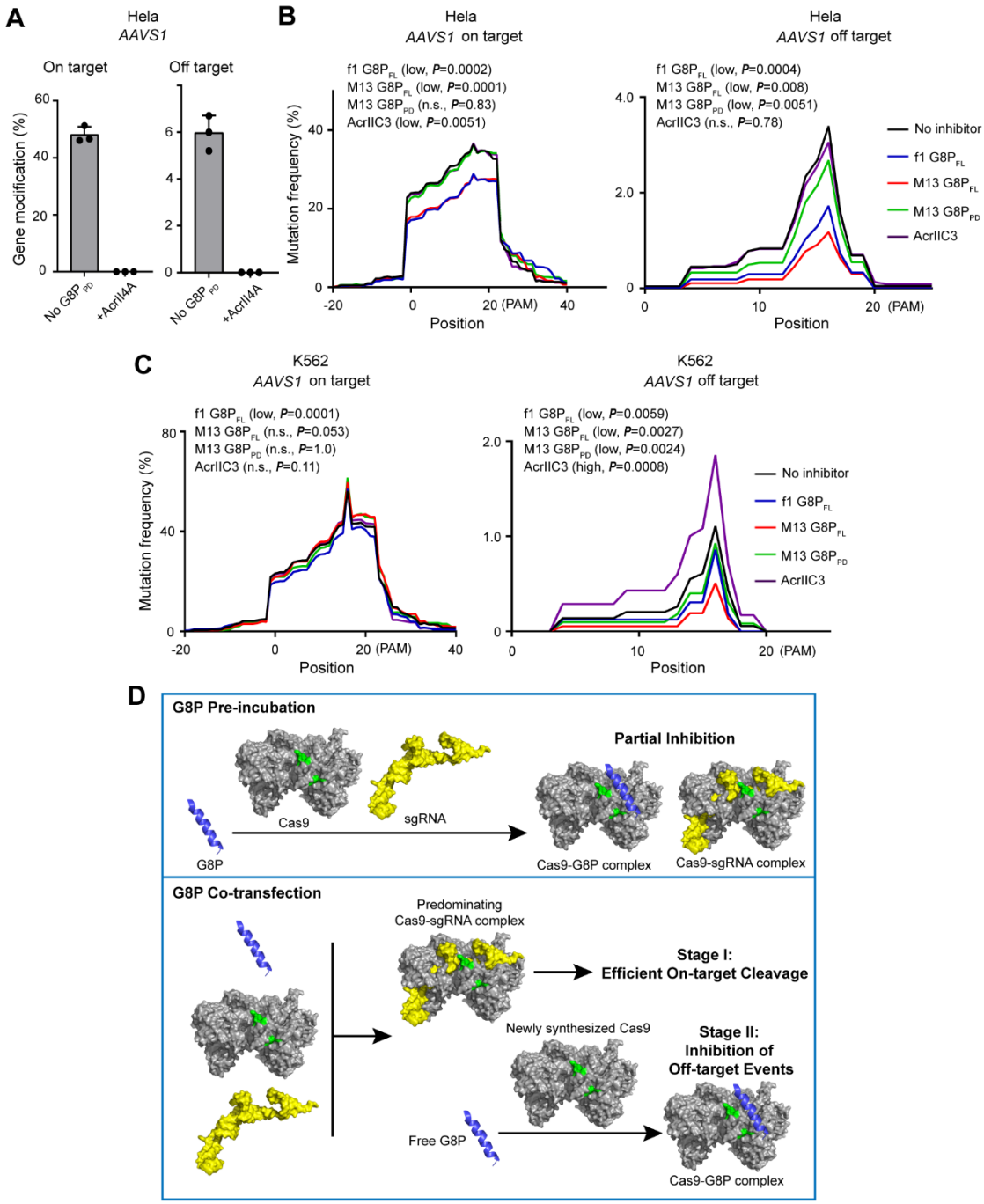

Figure 6. Analyses of the Effects of Co-transfected G8P and Acrs on the Genome-editing Activity of SpyCas9. (A) AcrII4A abolishes the on- and off-activities of SpyCas9, as determined by T7E1 assay. The results are shown as mean ± SD (n = 3). (B-C) Density plot showing the distribution of mutation rates along the gene-edited genomic sites of *AAVS1* in Hela (B) and K562 (C) cells. The mean value of three biological replicates are displayed. Significant difference between test groups and mock

is determined by one-way ANOVA with Dunnett's multiple comparisons test. Low and high indicates increased and decreased mutation rates, respectively. The adjusted *P* values are indicated. (D) Proposed mechanism of actions of G8P-mediated SpyCas9 suppression when delivered prior to or simultaneously with SpyCas9-coding genes.

STAR METHODS

KEY RESOURCES TABLE

REAGENT or RESOURCE	SOURCE	IDENTIFIER
Bacterial Strains		
Trelief™5α	TSINGKE	Cat# TSC01
VCMS13 Hepler phage	Stratagene	Cat# 200251
XL1-Blue	Agilent	Cat# 200228
BL21 (DE3) Plyss	TIAGEN	Cat# CB106-02
Chemicals and Recombinant Proteins		
PEG8000	Sangon Biotech	Cat# P0159-500G
LB Agar	Life technology	Cat# 22700-025
MOPS	AMRESCO	Cat# 0670-100G
Yeast Extract	OXOID	Cat# LP0021
Agarose	TSINGKE	Cat# TSJ001
Phanta Max Super-Fidelity DNA Polymerase	VAZYME	Cat# P505-d3
EcoRI-HF	NEB	Cat# R3101S
KpnI-HF	NEB	Cat# R3142S
XbaI	NEB	Cat# R0145V
BamHI-HF	NEB	Cat# R3136S
T7Endonuclease I	NEB	Cat# M0302L
ClonExpress Ultra one step Cloning Kit	VAZYME	Cat# C115-01
FETAL BOVINE SERUM	GIBCO	Cat# 10091148
Penicillin-Streptomycin	Sigma Aldrich	Cat# P4333
Poly-L-lysine	Meilunbio	Cat# MA0174
LIPOFECTAMINE 2000	GIBCO	Cat# 1166809
LIPOFECTAMINE 3000	GIBCO	Cat# 1946890
DMEM (Medium for mammalian cell culture)	GIBCO	Cat# 11995073
RPMI 1640	GIBCO	Cat# 11875119
Opti-MEM	GIBCO	Cat# 2003628
Phosphate Buffered Saline	Hyclone	Cat# SH30256
HEPES 1M Solution	Hyclone	Cat# SH30237.01
Deposited Data		
Mass spectrometry data	ProteomeXchange	Accession number: PXD012466.
NGS data	NCBI SRA	Accession number: SRP180801
Experimental Models: Cell Lines		
Human: HEK293T	ATCC	Cat# CRL-11268
Human: K562	SUERSEHNGWU	NA
Human: H1-Hela	ATCC	Cat# CRL-1958
Oligonucleotides		

Primers	TSINGKE	Table S1
Peptides	GeneScript	Figure S5
Recombinant DNA		
pET28b-spyCas9	Ian A.Wilson lab	NA
pcDNA3.1 (+)	Richard A.Lerner lab	NA
pST1374-SpyCas9	Xingxu Huang lab	NA
pGL-U6-gRNA	Xingxu Huang lab	NA
plv-EF1α-mCherry	Guang Yang lab	NA
Critical Commercial Assays		
MinElute PCR purification kit	QIAGEN	Cat# 28006
Endotoxin-free plasmid DNA purification	MACHEREY-NAGEL	Cat# 740422.50
Gel Extraction kit(100)	OMEGA	Cat# D2500-01
DNA Gel Extraction kit	TSINGKE	Cat# GE0101-50
Ni-NTA agarose	QIAGEN	Cat# 30210
VAHTS Universal DNA Library Prep Kit	Illumina	NA
SE Cell Line 4D-Nucleofector^{TM}X Kit S	LONZA	Cat#V4XC-1032
SF Cell Line 4D-Nucleofector^{TM}X Kit S	LONZA	Cat#V4XC-2032
HiScibe T7 Quick High yield RNA Synthesis kit	NEB	Cat# 10008100
Hiseq3000 SBS&Cluster kit	Genergy Biotech	Illumina HiSeq 3000 platform
ClonExpress Ultra One Step Cloning kit	VAZYME	Cat# C115-02
Software and Algorithms		
GraphPad Prism	GraphPad Prism Software	https://www.graphpad.com/scientific-software/prism/
ImageJ	ImageJ Software	https://imagej.nih.gov/ij/
HiSeq control	HiSeq Control Software	Illumina
Bowtie2	Bowtie2 Software	https://github.com/BenLangmead/bowtie2
Agilent 2100	Agilent 2100 Bioanalyzer	Agilent Technologies
Qubit2.0 fluorometer	Qubit2.0 Fluorometer	Invitrogen
VarScan v2.4	VarScan v2.4 Software	http://varscan.sourceforge.net/
SAMtools	SAMtools software	http://samtools.sourceforge.net/
Proteome Discoverer	Proteome Discoverer v 2.2 software	Thermo Scientific
Xcalibur v 3.0	Xcalibur v 3.0 Software	Thermo Scientific
XlinkX detect program	XlinkX detect program Software	Thermo Scientific

CONTACT FOR REAGENT AND RESOURCE SHARING

Further information and requests for resources and reagents should be directed to and will be fulfilled by the Lead Contact, Jia Liu (liujia@shanghaitech.edu.cn).

EXPERIMENTAL MODEL AND SUBJECT DETAILS

E. coli (XL1-Blue)

This bacterium line was used to produce M13 bacteriophage. XL1-Blue *E. coli* was grown at 37 °C in SB medium liquid or agar unless otherwise noted.

E. coli (BL21)

This bacterium line was used to produce Cas9 proteins. XL1-Blue *E. coli* was grown at 37 °C in LB medium liquid or agar unless otherwise noted.

M13 bacteriophage

To produce M13 phage, XL1-Blue *E. coli* was inoculated in SB medium supplemented with 2% glucose and grown until OD_{600} reached 0.5. M13 phages were transfected and incubated with XL1-Blue *E. coli* at 37 °C for 30 min and the culture was shaken at 37 °C for 1 h. Thereafter, bacteria were centrifuged twice at 3,000 rpm for 15 min at 4 °C and washed with SB medium to remove glucose and free phage particles. The cells were re-suspended with SB medium and diluted to an OD_{600} of 0.8 in 200 mL culture and grown at 30 °C overnight with shaking. The next day, the culture was centrifuged at 5,000 rpm for 15 min at 4 °C and the supernatant containing phage particles was collected. The

supernatant was gently mixed with NaCl-PEG buffer containing 20% PEG and 2.5 M NaCl and kept on ice for 1 h. The PEG-phage supernatant was centrifuged at 9,000 rpm for 30 min at 4 ℃. The supernatant was discarded and phage pellet was centrifuged again at 9,000 rpm for 5 min at 4 ℃ to remove residual medium. The precipitated phage particle was re-suspended in phosphate buffered saline (PBS) for further studies.

Cell culture

HEK293T cells were maintained in Dulbecco's Modified Eagle's medium (DMEM, Gibco/Thermo Fisher Scientific, Shanghai, China) supplemented with 10% fetal bovine serum (FBS, Gibco/Thermo Fisher Scientific) at 5% CO_2 and 37 °C in a fully humidified incubator and were passaged when 70-90% confluency was reached. K562 cells were cultured in RPMI-1640 medium supplemented with 10% FBS, 100 IU/mL of penicillin and 100 μg/mL of streptomycin at 37 °C under 5% CO_2. Cell lines were validated by VivaCell Biosciences (Shanghai, China).

METHOD DETAILS

Expression and purification of SpyCas9 proteins

pET28b plasmids coding SpyCas9 WT, K1158 mutant and K1176 mutant proteins were transformed into *E. coli* BL21 (DE3) cells. Single colonies were picked and grown in 2 liter LB media supplemented with 50 μg/mL kanamycin. Culture was grown to an OD_{600} of 0.8. Protein expression was induced with 0.2 mM isopropyl-β-D-thiogalactopyranoside (IPTG) at 16 °C overnight. Cells from 2 liter culture were

pelleted by centrifugation at 6,000 g at 4 °C for 15 min and then re-suspended in 40 mL binding buffer containing 20 mM TrisHCl, pH 8.0 and 0.5 M NaCl. Cell suspension was then supplemented with 1 mM Tris (2-carboxyethyl) phosphine (TCEP) and 1× complete inhibitor cocktail (Roche). Cells were lysed by sonication on ice and then centrifuged at 80,000 g at 4 °C for 30 min. The supernatant of cell lysate was incubated with 1 mL Ni-NTA agarose beads (QIAGEN) at 4 °C for 1 h. The resin was washed with 20 mL wash buffer that was made by supplementing binding buffer with 30 mM imidazole. Proteins were eluted with 5 mL elute buffer that was made by supplementing binding buffer with 300 mM imidazole. Eluted protein samples were further purified by gel filtration using Superose 6 10/300 column (GE Healthcare). These proteins were buffer-exchanged to storage buffer containing 20 mM HEPES, pH 8.0 and 200 mM NaCl, aliquoted and stored at -80 °C.

Construction of G8P$_{PD}$ overexpression plasmids

Human codon-optimized DNA sequences encoding M13, f1, f1 mutant 2 and pf1 G8P$_{PD}$ were cloned into the BamHI/XbarI sites of pcDNA3.1(+) by plasmid recombination kit Clone Express (Vazyme). These G8P$_{PD}$ peptides carry an N-terminal SV40 nuclear localization signal (NLS) for co-localization with Cas9 proteins. G8P$_{PD}$ peptides were cloned into plv-EF1α-mCherry plasmid harboring mCherry fluorescent protein marker. sgRNA was cloned into pGL3-U6-gRNA plasmid carrying green fluorescent protein (GFP).

In vitro transcription of sgRNA

sgRNA was transcribed from a sgRNA-coding PCR product with a 5′ T7 promoter sequence using HiScibe T7 Quick High yield RNA Synthesis kit (NEB). The transcription was performed at 37 °C overnight and then purified by phenol: chloroform extraction, followed by ethanol precipitation. Purified sgRNA was quantified by spectrometry and stored at -80 °C.

In vitro cleavage assay

Cas9 protein and transcribed sgRNA were incubated for 10 min at room temperature in reaction buffer containing 1× NEB buffer 3.1 (NEB Biolabs) supplemented with 1 mM DTT) to form Cas9-sgRNA RNP complex. Cleavage was performed in 10 μL reactions containing 100 ng of substrate DNA and 1 μL RNP complex of indicated concentrations at room temperature for 1 h. Reactions were terminated by addition of 1× DNA loading buffer and resolved on 2% agarose gels. For inhibition experiments, $G8P_{PD}$ peptides were dissolved in deionized distilled water and incubated with Cas9 protein or pre-assembled Cas9-sgRNA RNP for 10 min at room temperature and the mixed solution was then added to the *in vitro* cleavage reaction. For experiments comparing the inhibitory activities of $G8P_{PD}$ peptides, 0.1% dimethyl sulfoxide (DMSO) was included in the reaction solution to solubilize lyophilized peptide samples.

Electrophoresis mobility shift assay (EMSA)

sgRNA concentration is fixed to 15 μM and Cas9 protein was titrated with a molar ratio

of Cas9 over sgRNA ranging from 0.05 to 1. f1 $G8P_{PD}$ of 150, 300 and 600 μM was incubated with Cas9 protein or pre-assembled Cas9-sgRNA RNP complex for 20 min at 25 °C and quenched by addition of 1× native DNA loading buffer containing 40 mM Tris, pH 8.2, 40 mM acetate, 1 mM ethylenediaminetetraacetic acid (EDTA), 12.5% (v/v) glycerol, 0.025% (m/v) bromophenol blue. The samples were run on 2% agarose gels. For the order-of-addition experiment, Cas9 and sgRNA concentrations are fixed to 7.5 and 15 μM respectively. SpyCas9 was pre-incubated with sgRNA or $G8P_{PD}$ for 20 min, followed by incubation with the counterpart for 20 min at 25 °C.

Chemical crosslinking and mass spectrometry

Cas9 protein and M13 $G8P_{PD}$ were crosslinked using collision-induced dissociation (CID)-cleavable cross-linker-disuccinimido sulfoxide (DSSO) following the described procedure (Kao et al., 2011) with minor modification. Cas9 protein and peptides were mixed in PBS and incubated for 30 min at room temperature. Crosslinking was performed for 30 min by adding DSSO (Thermo Scientific) to protein/peptide solution with 1,000 molar excess. The crosslinking reaction was quenched by excess Tris and the crosslinked products were digested with Chymotrypsin. The LC MSn data of digested peptides were collected on Orbitrap Fusion Tribrid (Thermo Scientific) with an on-line NanoLC system and analyzed using CID-MS^2-MS^3 strategy as previously described (Liu et al., 2017). Monoisotopic mass of parent ions and corresponding fragment ions, parent ion charge states and ion intensities from LC MS^2 and LC MS^3 spectra were extracted using Xcalibur v 3.0 (Thermo Scientific). Database searching

was performed using Proteome Discoverer v 2.2 software (Thermo Scientific). Chymotrypsin was set as the enzyme with two missed cleavages being allowed as the maximum values. Protein N-terminal acetylation, methionine oxidation (15.995 Da), carbamidomethyl cysteine (57.021 Da), hydrolyzed lysine DSSO (176.014 Da) and lysine DSSO TRIS (279.078 Da) were selected as variable modifications. In addition, to account for the residual crosslinker three defined modifications on uncleaved lysines were chosen including alkene (C_3H_2O, 54 Da), sulfenic acid ($C_3H_4O_2S$,104 Da) and thiol (C_3H_2SO, 86 Da) modifications. A false discovery rate (FDR) of 1% was employed to filter out false positive results. The MS, MS^2 and MS^3 mass tolerances were set as 10 ppm, 20 ppm and 0.6 Da respectively.

The XlinkX detect program (Thermo Scientific) was used to search MS^2 data and identify the list of putative DSSO-interlinked products based on their unique DSSO fragmentation patterns. Monoisotopic masses and charges of parent ions measured in MS^3 scans for those putative cross-linked peptides were further validated and scored by XlinkX. The final results were confirmed by manual inspection of the MS^2 and MS^3 spectra, respectively.

Circular dichroism

Circular dichroism spectroscopy (Chirascan-plus CD spectrometer, Applied Photophysics) was used to probe the peptide conformational changes. 100 μM WT and mutant 2 $G8P_{PD}$ peptides were dissolved in deionized water. The CD data were recorded at 25 ^{o}C and the average value of three biological replicates was presented.

Inhibition of CRISPR-Cas9 activity in human cells by G8P$_{PD}$ overexpression

K562 cells (2×10^5) were harvested, washed with PBS and re-suspended in 20 μL of SF nucleofection buffer (Lonza). G8P$_{PD}$-coding plasmid (1 μg) was mixed with re-suspended K562 cells and nucleofected by Lonza 4D nucleofector with program FF-120. Immediately following the nucleofection, 100 μL pre-warmed RPMI-1640 medium was added into nucleofection cuvettes and the cells were transferred to culture dishes. At 24 post nucleofection, plasmids encoding SpyCas9 (500 ng) and *AAVS1* or *EMX1*-targeting sgRNA (250 ng) were transfected into G8P$_{PD}$-expressing K562 cells by nucleofection as described above.

Low-passage HEK293T cells were seeded into 24-well plates at a density of 150,000 cells per well. The next day, G8P$_{PD}$ plasmid (1 μg) were transfected into cells using Lipofectamine 3000 (Invitrogen). At 24 h post G8P$_{PD}$ transfection, plasmids encoding SpyCas9 (0.5 μg) and *AAVS1*-targeting sgRNA (250 ng) were co-transfected into G8P$_{PD}$-expressing HEK293T cells. For co-transfection experiments, K562 and Hela cells were nucleofected with 1 μg of G8P$_{PD}$ plasmid, 0.5 μg of SpyCas9 plasmid and 0.5 μg sgRNA plasmid.

At 48 h after transfection of SpyCas9 and sgRNA plasmids, mCherry and GFP dual positive cells were collected using a BD FACSAria III flow cytometer (BD Biosciences). At least 2,000 cells were collected for subsequent analyses. The genomic DNA of sorted cells was extracted using QuickExtract DNA Extraction Solution (Epicentre). Genomic PCR reaction was performed using 100 ng genomic DNA,

corresponding primers (Supplementary Table 1), Phanta Max Super-fidelity DNA Polymerase (Vazyme) or KOD plus (Takara) using a touchdown cycling protocol (30 cycles of 98 °C for 10 s, 68-58 °C for 15 s and 68 °C for 60 s). The PCR products were digested by T7E1 enzyme (NEB), resolved on 2% agarose gel and then analyzed by densitometry measurements as described (Guschin et al., 2010). Three biological replicates were performed for each condition.

Next-generation sequencing of edited genomic sites

Genomic DNA (100 ng) from *AAVS1*-edited K562 cells was subject to PCR reactions using stubbed primers (Supplementary Table 1). PCR products were purified using Gel Extraction Kit (OMEGA). A high-throughput library preparation kit (Hiseq3000 SBS&Cluster kit) was used to generate dual-indexed sequence. Two or three biological replicates were processed by Genergy Biotech (Shanghai, China) or Genewiz (Suzhou, Jiangsu, China) using Illumina HiSeq 3000 platform.

Next generation sequencing library preparations were constructed following the manufacturer's protocol (VAHTS Universal DNA Library Prep Kit, Illumina). For each sample, more than 50 ng purified PCR fragment was used for direct library preparation. The fragments were treated with End Prep Enzyme Mix for end repairing, 5′ phosphorylation and dA-tailing in one reaction, followed by a T-A ligation to add adaptors to both ends. Size selection of adaptor-ligated DNA was then performed using VAHTSTM DNA Clean Beads. Each sample was then amplified by PCR for 8 cycles using P5 and P7 primers. Both P5 and P7 primers carry sequences that can anneal with

flowcell to perform bridge PCR. In addition, P7 primer carries a six-base index allowing for multiplexing. The PCR products were cleaned up using VAHTSTM DNA Clean Beads, validated using an Agilent 2100 Bioanalyzer (Agilent Technologies, Palo Alto, CA, USA) and quantified by Qubit2.0 Fluorometer (Invitrogen, Carlsbad, CA, USA). Then libraries with different indexes were multiplexed and loaded on an Illumina HiSeq instrument according to manufacturer's instructions (Illumina, San Diego, CA, USA). Sequencing was carried out using a 2 x 150 paired-end (PE) configuration. Image analyses and base calling were conducted by the HiSeq Control Software (HCS) + OLB + GAPipeline-1.6 (Illumina) on the HiSeq instrument. Sequencing reads were obtained in the Fastq format.

Amplicons with less than 6 M read counts were excluded from the analyses. Short reads were aligned to the reference sequence by Bowtie2 (Langmead and Salzberg, 2012) with the following parameters: -D 5 -R 3 -N 1 --gbar 1 --rdg 5,1 --rfg 5,1 --dovetail. Aligned reads were sorted by SAMtools (Li et al., 2009) and INDEL and SNP calling was performed by mpileup (Li and Durbin, 2009) with maximum read depth per sample equal to the total reads mapped. VarScan v2.4 (Koboldt et al., 2012) was used for the quality control of SNPs and INDELs in mpileup output with a minimum variant frequency of ≥ 0.001, and a *P* value threshold of ≤ 0.05. With the above settings, the following items were quantified including the proportions of reads with INDELs/SNPs at each position in the 20 bp target region, the proportions of INDEL with different insertion or deletion length, the proportions of INDEL reading frames (3N, 3N+1 and 3N+2) and the proportions of reads harboring variants over the total number of aligned

reads.

QUANTIFICATION AND STATISTICAL ANALYSES

Two or three biological replicates were performed for each experimental condition. Significant difference was analyzed using one-way ANOVA with Dunnett's multiple comparisons test unless otherwise noted.

DATA AND SOFTWARE AVAILABILITY

The mass spectrometry data have been deposited into ProteomeXchange with the accession number PXD012466. Deep sequencing data have been deposited into NCBI SRA database with the accession number SRP180801. Additional data that support the findings of this study are available from the lead contact author J. Liu upon request.

Supplemental Information

Precision Genome Editing Using Bacteriophage-derived Peptides

Yan-ru Cui[1,4,5], Shao-jie Wang[1,5], Jun Chen[2], Jie Li[1,4], Wenzhang Chen[1], Shuyue Wang[1], Bing Meng[1], Wei Zhu[1], Zhuhong Zhang[3], Bei Yang[1], Biao Jiang[1], Guang Yang[1], Peixiang Ma[1,*], Jia Liu[1,6*]

[1]Shanghai Institute for Advanced Immunochemical Studies, ShanghaiTech University, Shanghai, 201210, China.

[2]College of Life Sciences, Zhejiang University, Hangzhou, Zhejiang, 310058, China.

[3]School of Pharmacy, Key Laboratory of Molecular Pharmacology and Drug Evaluation (Yantai University), Ministry of Education, Collaborative Innovation Center of Advanced Drug Delivery System and Biotech Drugs in Universities of Shandong, Yantai University, 264005, Yantai, Shandong, People's Republic of China.

[4]University of Chinese Academy of Sciences, Beijing, China.

[5] These authors contributed equally to this work.

[6]Lead Contact

*Correspondence: J.L. (liujia@shanghaitech.edu.cn) and P.M. (mapx@shanghaitech.edu.cn)

TABLE OF CONTENT

1. **Supplemental Figures**
2. **Supplemental Tables**
3. **Supplemental Experimental Procedures**

Supplemental Figures

Figure S1. Comparison of M13 and f1 Phage G8P$_{PD}$. (A) Sequence alignment of M13 and f1 G8P$_{PD}$. (B) The *in vitro* Cas9-inhibiting activity of M13 and f1 G8P$_{PD}$. M13 and f1 G8P$_{PD}$ of 100 μM were incubated with 50 nM of Cas9 proteins prior to the addition of 50 nM of sgRNA.

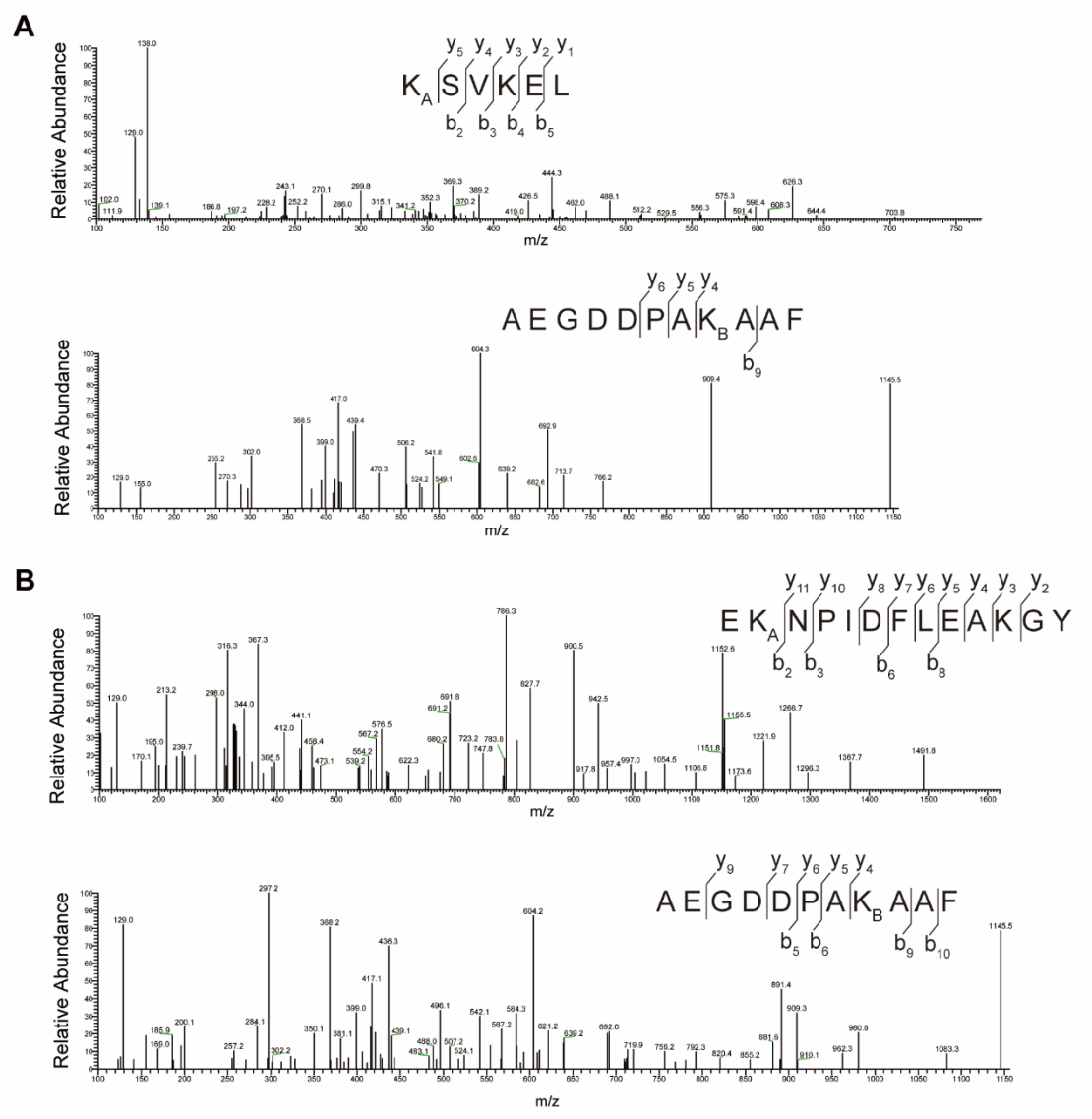

Figure S2. MS Analyses of the Interface between SpyCas9 and M13 G8P$_{PD}$. (A) Tertiary MS for individual peptides KSVKEL and AEGDDPAKAAF as described in Figure 3B. (B) Tertiary MS for individual peptides ENKPIDFLEAKGY and AEGDDPAKAAF as described in Figure 3C.

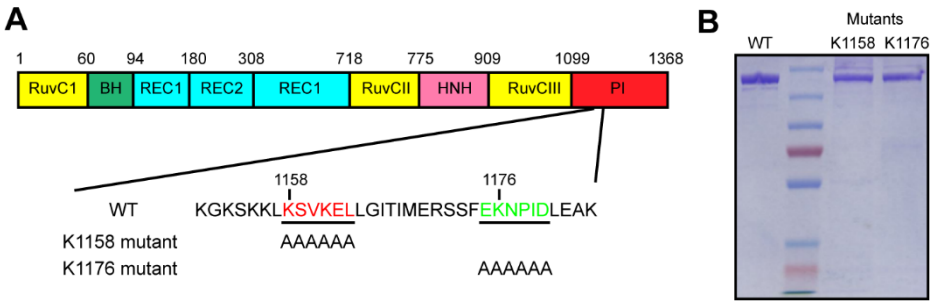

Figure S3. Construction and Purification of SpyCas9 K1158 and K1176 Mutants. (A) Schematic presentation of the structural organization of *S. pyogenes* Cas9. BH, bridging helix. PI, PAM interacting domain. Positions of alanine mutations in K1158 and K1176 mutants are indicated. (B) Purified WT, K1158 mutant and K1176 mutant SpyCas9 proteins.

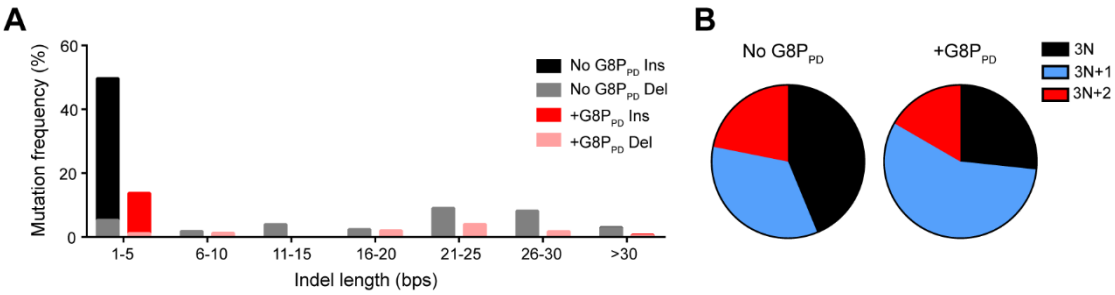

Figure S4. Profile of SpyCas9-induced Mutations in the Absence and Presence of G8PPD. (A) Distribution of indel length. (B) Distribution of indel frame phase calculated as the length of indels modulus. The mean value of two biological replicates are shown.

Organism	Uniprot ID	Bacteria Host	Peptide Sequence
Enterobacteria phage M13	P69541	*Escherichia coli*	AEGDDPAKAAFNSLQASATEY
Pseudomonas phage Pf1	P03621	*Pseudomonas aeruginosa*	ATSLPAFAGVIDTSAVESAITDGQGDMKA
Enterobacteria phage f1	P69540	*Escherichia coli*	AEGDDPAKAAFDSLQASATEY
Pseudomonas phage Pf3	P03623	*Pseudomonas aeruginosa*	MQSVITDVTGQLTAVQAD
Enterobacteria phage IKe	P03620	*Escherichia coli*	AEPNAATNYATEAMDSLKTQAIDLI
Enterobacteria phage If1	P03619	*Escherichia coli*	ADDATSQAKAAFDSLTAQATEM
Xanthomonas phage Xf	P03622	*Xanthomonas campestris* pv. oryzae	SGVGDGVDVVSAIEGAAGP
Thermus phage PH75	P82889	*Thermus thermophilus*	MDFNPSEVASQVTNYIQ
Enterobacteria phage I2-2	P15416	*Escherichia coli*	ADDGTSTATSYATEAMNSLKTQATDLIDQ
Xanthomonas phage phiLf	P68674	*Xanthomonas campestris* pv. campestris	MGDILTGVSGAE

Figure S5. G8P$_{PD}$ Peptides Derived from Inoviridae Bacteriophages.

Supplementary Tables

Table S1. Primer list.

Name	Use	Sequence
CCR5-Ext-FWD	Forward external primer for PCR cleavage template	aggtgagaggattgcttg
CCR5-Ext-REV	Reverse external primer for PCR cleavage template	aaatgagagctgcaggtg
CCR5-Int-FWD	Forward internal primer for PCR cleavage template	gagccaagctctccatctagt
CCR5-Int-REV	Reverse internal primer for PCR cleavage template	gccctgtcaagagttgacac
AAVS1-NGS-FWD	NGS, Forward	tctttccctacacgacgctcttccgatctc tggtgacacacccccattt
AAVS1-NGS-REV	NGS, Reverse	gtgactggagttcagacgtgtgctcttc cgatctccaggatcagtgaaacgcac
AAVS1-Ext-FWD	Forward external primer for nested PCR for T7E1 assay	ggagttttccacacggacac
AAVS1-Ext-REV	Reverse external primer for nested PCR for T7E1 assay	cccctatgtccacttcagga
AAVS1-Int-FWD	Forward internal primer for nested PCR for T7E1 assay	tgcttctcctcttgggaagt
AAVS1-Int-REV	Reverse internal primer for nested PCR for T7E1 assay	cggttaatgtggctctggtt
EMX1-FWD	Forward primer for T7E1 assay	ggagcagctggtcagagggg
EMX1-REV	Reverse primer for T7E1 assay	gggaagggggacactgggga

Table S2. sgRNA-targeted genomic sites in this study.

Gene	Sequence
EMX1	gagtccgagcagaagaagaaggg
AAVS1	gggagggagagcttggcagg